ACS APPLIED MATERIALS & INTERFACES

Research Article

www.acsami.org

Violet Emission in ZnO Nanorods Treated with High-Energy Hydrogen Plasma

Cong Chen, Yangfan Lu, Haiping He, Mu Xiao, Zheng Wang, Lingxiang Chen, and Zhizhen Ye*

State Key Laboratory of Silicon Materials, Department of Materials Science and Engineering, Zhejiang University, Hangzhou 310027, People's Republic of China

Supporting Information

ABSTRACT: Violet photoluminescence was observed in high-energy hydrogen-plasma-treated ZnO nanorods at 13 K. The photoluminescence spectrum is dominated by a strong violet emission and a shoulder attributed to excitonic emission. The violet emission shows normal thermal behavior with an average lifetime of about 1 μs at 13 K. According to the time-resolved and excitation density-dependent photoluminescence, it was found that the violet emission is determined by at least two emitting channels, which was confirmed by annealing experiments. Evidence was also given that the violet emission is related to hydrogen. We suggested that the hydrogen-related complex defects formed under high-energy hydrogen plasma treatment are responsible for this violet emission.

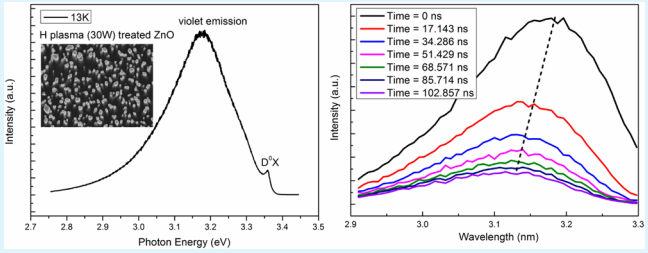

KEYWORDS: *ZnO nanorods, hydrogen plasma, photoluminescence, violet emission, TRPL, hydrogen-related complex defects*

INTRODUCTION

Wurtzite ZnO offers some fascinating properties, including a direct wide band gap (~3.37 eV) and a large exciton binding energy (~60 meV).[1,2] This binding energy allows the stable existence of excitons at room temperature. One-dimensional (1D) ZnO nanostructures have received great attention in the past decade because of their unique optical and electrical properties.[3] Nowadays, the potential application of ZnO has been hindered by the difficulty in understanding and controlling the electrical and optical properties of native point and extended structural defects such as interstitials, vacancies, dislocations, and stacking faults.[4] Photoluminescence (PL) is a very sensitive and nondamaging tool for the study of defects in semiconductors. Features of the emission spectrum can provide information on the band structure and thus be exploited to identify surface, interface, and impurity levels. At low temperatures, the native point defects can also create radiative channels and may lead to the appearance of new emission lines. The PL properties of ZnO have been extensively studied in recent years. Because of the large surface-to-volume ratio, surface states play important roles in the PL properties of ZnO nanostructures. To improve the PL properties of ZnO, various surface modifications such as ion implantation,[5] Argon (Ar)-ion milling,[6] metal capping,[7,8] and hydrogen (H) plasma treatment[9,10] have been demonstrated. Moreover, various annealing treatments have also been used to enhance the optical properties of ZnO.[11−13]

Very recently, low-energy H plasma treatment with a power of 20 W has been used for ZnO nanorods, and it was shown that the treated ZnO exhibited enhanced optical properties due to surface passivation and H doping.[14] In this work, the as-grown ZnO nanorods were subjected to high-energy H plasma treatment with a power of 30 W, and it was shown that the treated sample exhibited unusual PL features. The PL spectrum at 13 K is dominated by an extremely strong violet emission around 3.18 eV with an average lifetime of about 1 μs and a shoulder attributed to excitonic emission at 3.36 eV. Such a dominant violet emission has rarely been observed in ZnO. The annealing experiments give evidence that the violet emission is related to H. On the basis of our results, we suggested that H-related complex defects formed under high-energy H plasma treatment are responsible for this violet emission. The present results can promote our understanding of the impact of defects on the optical properties of ZnO nanostructures.

EXPERIMENTAL SECTION

ZnO nanorods were grown on a Si(100) substrate via a vapor-transport method in a horizontal quartz tube furnace by two steps. First, 100-nm-thick ZnO seed layers were deposited on the Si(100) substrate by radio-frequency magnetron sputtering from a ZnO target at 450 °C, with the sputtering power kept at 150 W. Then the substrate, together with zinc powder used as the zinc source, was placed in the furnace tube. Ar was used as the carrier gas. The growth temperature was set at 600 °C, and the working pressure was maintained at 10^{-1} Torr. H plasma treatments for the as-grown ZnO nanorods were performed in a direct-current plasma for 40 min at room temperature. The plasma power was set at 20−35 W, and the pressure was set at 10 mTorr.

Received: July 30, 2013
Accepted: September 25, 2013
Published: September 25, 2013

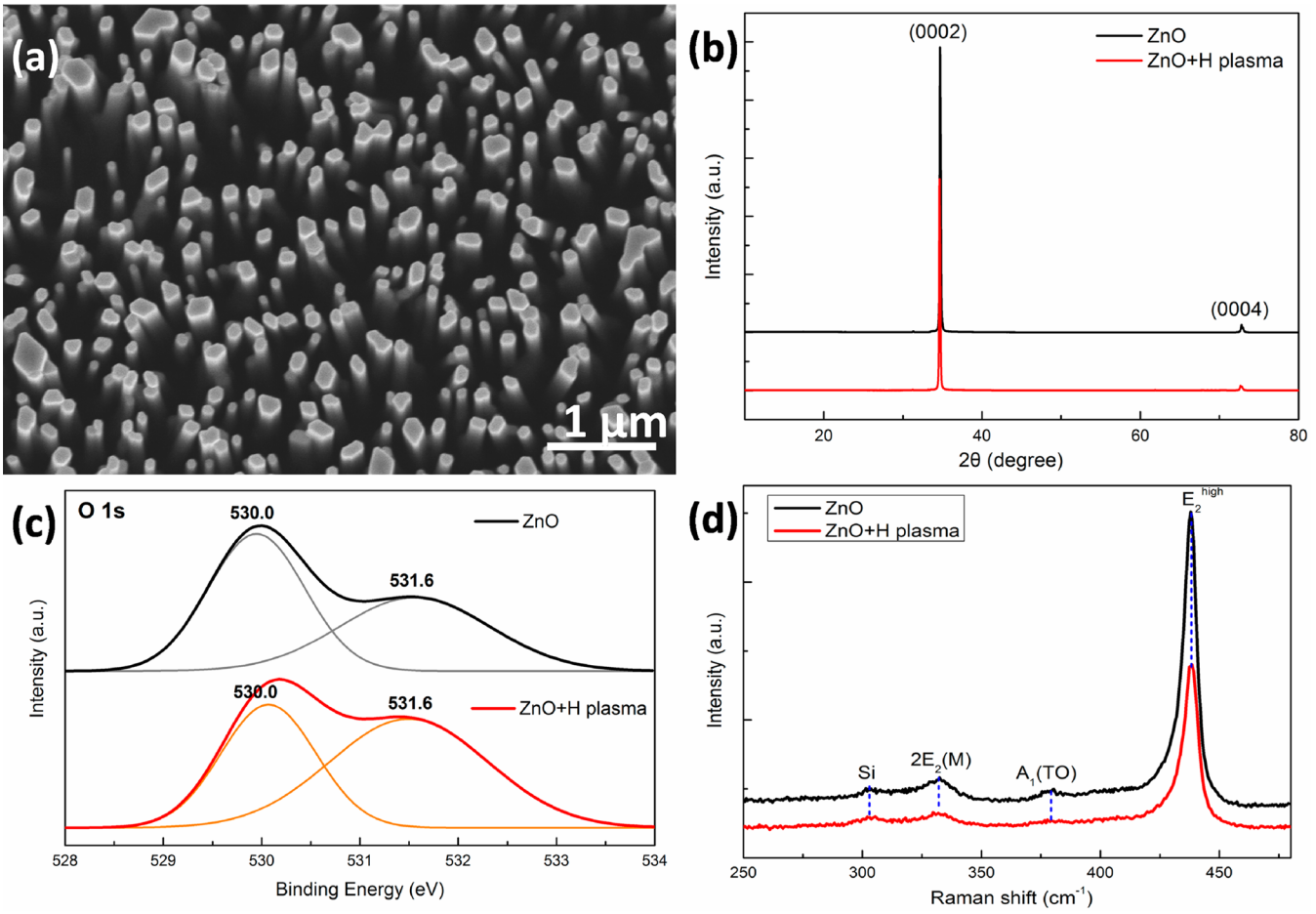

Figure 1. (a) FESEM image of the as-grown ZnO nanorods. (b) XRD spectra of the as-grown and H-plasma-treated (30 W) ZnO nanorods. (c) O 1s XPS spectra of the as-grown and H-plasma-treated (30 W) ZnO. (d) Raman spectra of the as-grown ZnO and H-plasma-treated (30 W) ZnO.

The morphologies and structures of the samples were characterized by field-emission scanning electron microscopy (FESEM; Hitachi S4800), X-ray diffraction (XRD; Bede D1) with Cu Kα radiation (λ = 0.15406 nm), and Raman spectroscopy (Jobin Yvon HR-800, Ar^+ laser, 514 nm). The changes of the chemical states of ZnO after H plasma treatment were recorded by X-ray photoelectron spectroscopy (XPS). The measurements were performed on a Thermo ESCALAB 250 system with a monochromatic Al Kα ($h\nu$ = 1486.6 eV) X-ray source. The outer layers of the samples were peeled off by Ar^+-ion sputtering for durations of 1 min. PL spectra were recorded on a FLS920 fluorescence spectrometer (Edinburgh Instruments) with a 325 nm helium−cadmium laser as the excitation source equipped with a variable attenuator. PL measurements were conducted at temperatures ranging from 13 to 300 K with a closed-cycle helium cryostat. Time-resolved PL (TRPL) were excited by a picosecond pulsed light-emitting diode with a pulse width of 881.4 ps and a pulsed period of 10 μs.

RESULTS AND DISCUSSION

Figure 1a shows the SEM image of the as-grown ZnO nanorods with average diameter of ~100 nm, which possess well-defined top facets. After high-energy (30 W) H plasma treatment, the morphology of the nanorods does not change much (not shown here). The XRD pattern of the as-grown ZnO nanorods in Figure 1b illustrates that these nanorods are wurtzite-type with [0001] as the preferred growth direction, which is similar to the XRD pattern of the H-plasma-treated sample. Figure 1c shows the O 1s XPS spectra of the as-grown and H-plasma-treated ZnO. It has been reported that the peak at a binding energy of 530.0 eV should be attributed to Zn−O−Zn,[15] and the peak at a binding energy of 531.6 eV could be attributed to Zn−O−H.[16] A much stronger peak at 531.6 eV was obtained in a H-plasma-treated sample by Gaussian fitting, indicating the incorporation of H into ZnO. In the Raman spectra in Figure 1d, besides the signal from the silicon substrate, all of the other peaks can be assigned to the intrinsic Raman modes of ZnO ($2E_2$(M) at ~332 cm^{-1}, A_1(TO) at ~379 cm^{-1}, and E_2^{high} at ~438 cm^{-1}).[17,18] No silent Raman modes originating from structural perturbation in ZnO were observed, indicating that not many structural defects were induced by the incorporation of H during the H plasma treatment.

Figure 2a shows the room-temperature PL spectra of ZnO nanorods before and after high-energy (30 W) H plasma treatment. The as-grown sample showed a near band emission (NBE) and a broad visible emission. There is still no consensus on the PL mechanism of the visible emission. Many researchers suggested that bulk defects such as oxygen vacancies are responsible for the visible emission.[19] Some researchers also suggested that the surface states of ZnO nanostructures can contribute to the visible emission.[20] However, after H plasma treatment, the NBE was greatly enhanced by ~100 times, while the visible emission was totally quenched. It is believed that both surface states and native defects can be passivated by H, leading to suppression of the visible emission. Similar observations were reported by us recently.[14] In addition, both

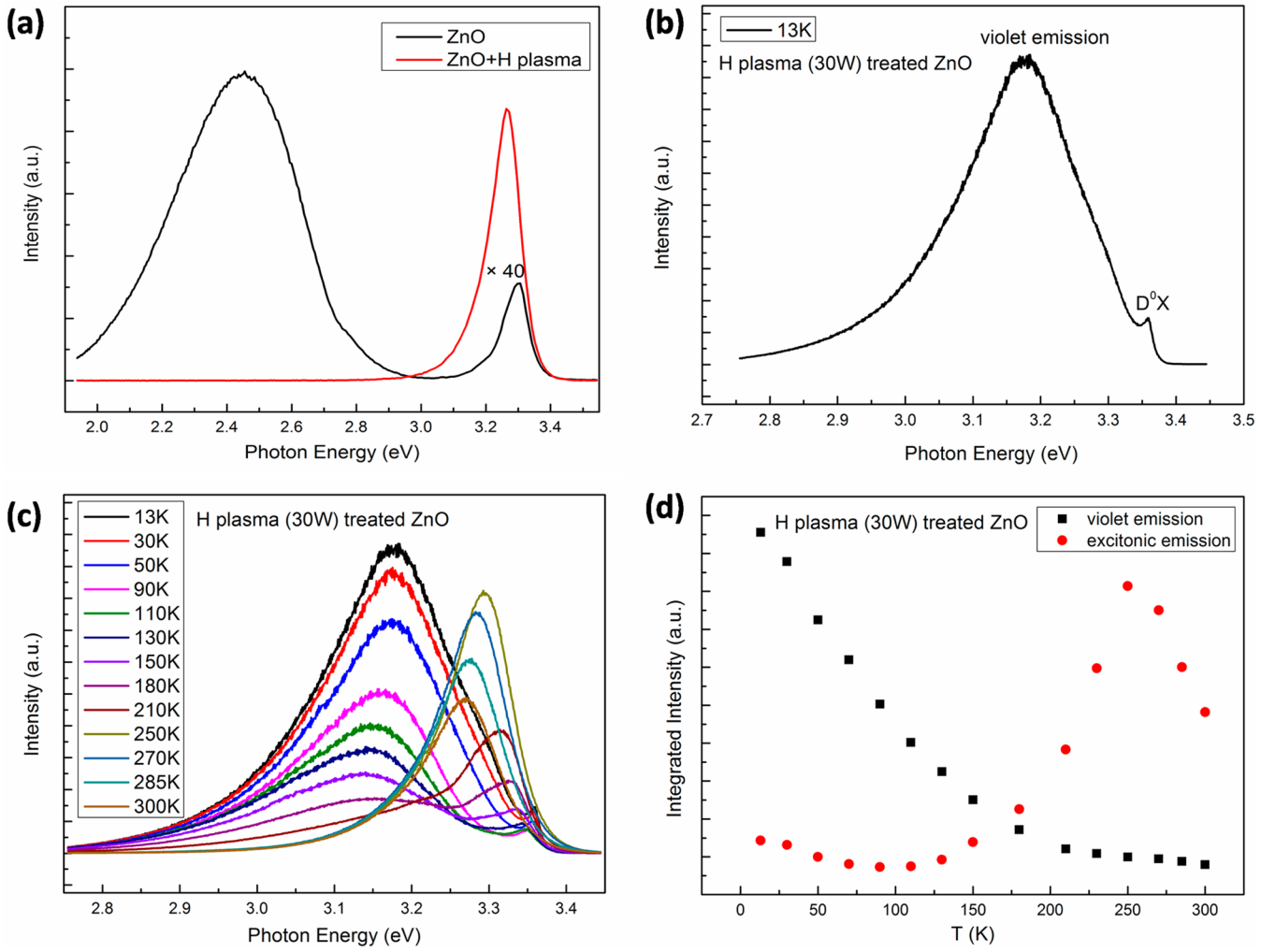

Figure 2. (a) Room-temperature PL spectra of the as-grown and H-plasma-treated (30 W) ZnO nanorods. (b) Low-temperature PL spectrum of the ZnO nanorods treated by H plasma (30 W) at 13 K. (c) Temperature-dependent PL spectra of the ZnO nanorods treated by H plasma (30 W). (d) Integrated intensities of the violet and excitonic emission as a function of the temperature for a H-plasma-treated (30 W) sample.

the passivation of nonradiative recombination centers and H doping are responsible for NBE enhancement.[21]

Figure 2b shows the low-temperature (13 K) PL spectrum of the H-plasma-treated ZnO nanorods. The H-plasma-treated sample exhibited an interesting feature: a dominant violet emission around 3.18 eV and a shoulder at 3.36 eV. The 3.36 eV line is attributed to the neutral-donor-bound exciton emission (D^0X). Such a feature is quite different from those commonly observed in normal ZnO nanorods. As a comparison, the PL spectrum of the nanorods without H plasma treatment is also given, showing a dominant peak at 3.35 eV, which is also attributed to D^0X (Figure S1 in the Supporting Information, SI). Figure 2c shows the temperature-dependent PL spectra of the H-plasma-treated ZnO nanorod. Interestingly, the excitonic emission shows negative thermal quenching (NTQ) behavior within a temperature range from 110 to 250 K, and the violet emission shows normal thermal quenching behavior. The NTQ behavior of the excitonic emission is more clearly seen in Figure 2d. The NTQ behavior that the PL intensity increases with increasing temperature within a certain temperature range has been observed in many semiconductors, including ZnO, which can be explained by the release of carriers/excitons from localized or trap states.[22−24] However, such NTQ behavior within such a large temperature range was rarely reported before. In addition, the excitonic emission of the as-grown ZnO nanorods shows normal thermal quenching behavior (Figure S2 in the SI). Interestingly, when the plasma power was reduced to 20 W, the sample showed only one dominant peak at 3.34 eV, which also showed the normal thermal quenching behavior (Figures S3 and S4 in the SI). It can be seen that the violet emission here only exists in ZnO nanorods treated with high-energy H plasma. Moreover, it seems that the NTQ behavior does not appear when there is no violet emission. However, the mechanisms for the NTQ behavior of the excitonic emission here are beyond the scope of this work and need further studies.

To study the origin of the violet emission, transients on the violet emission were measured at different temperatures, as shown in Figure 3a. The data can be fitted with the biexponential decay

$$I(t) = A_1 \exp(-t/\tau_1) + A_2 \exp(-t/\tau_2) \quad (1)$$

where I is the luminescence intensity, τ is the lifetime, and A is the constant. For comparison, the average lifetime, $\langle\tau\rangle = (A_1\tau_1^2 + A_2\tau_2^2)/(A_1\tau_1 + A_2\tau_2)$, was also calculated.[25] The fitting results are listed in Table 1. At 13 K, the average lifetime of about 1 μs can be obtained. It can also be seen that the lifetime decreases with increasing temperature significantly. According to TRPL

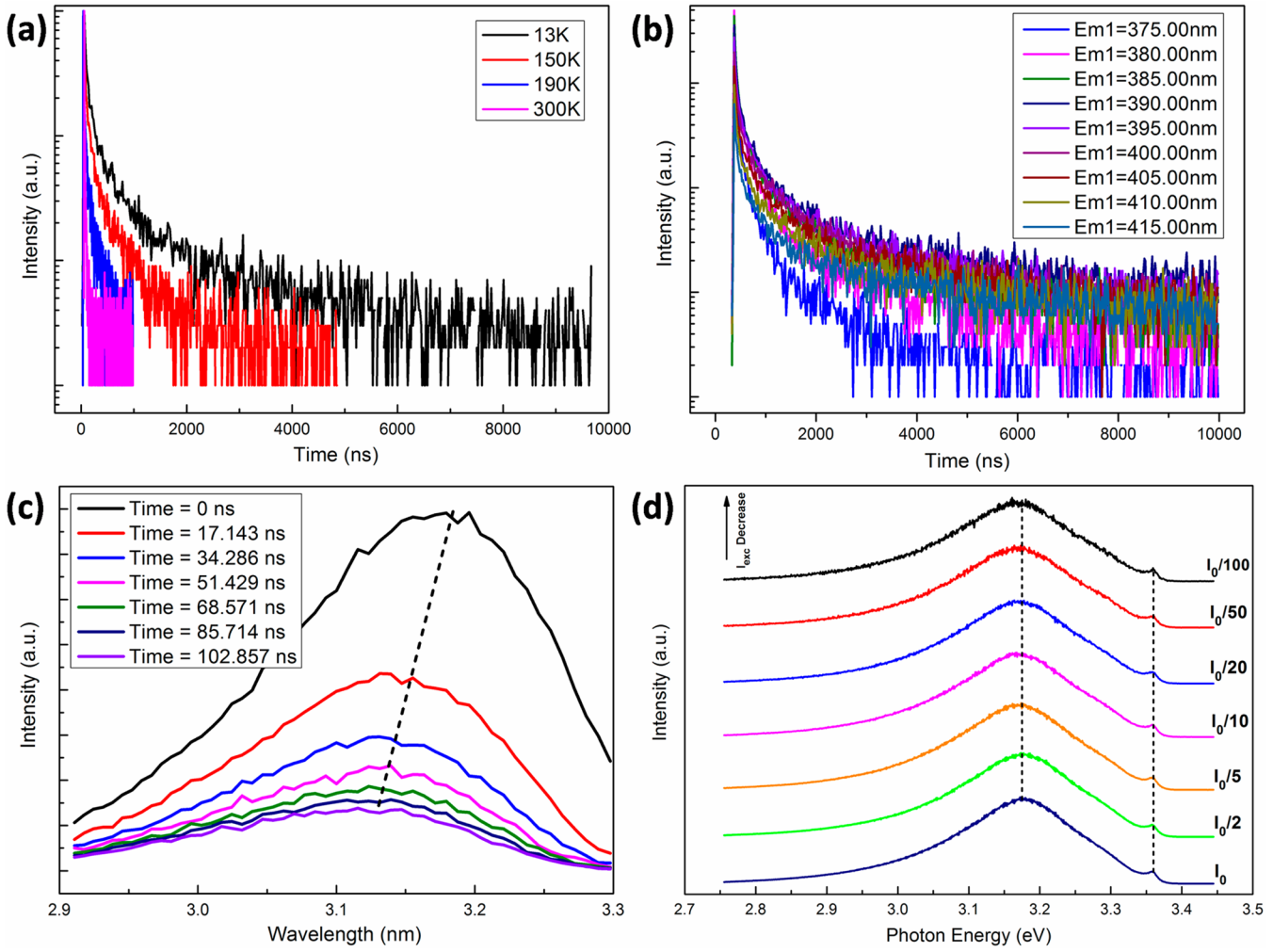

Figure 3. (a) Decay curves of the violet emission in H-plasma-treated (30 W) ZnO nanorods at different temperatures. (b) TRPL at different peaks of the violet emission at 13 K. (c) Red-shift trend of the PL peak from 3.18 to 3.13 eV with the delay time, obtained by TRPL analyses. (d) Excitation density-dependent PL spectra at 13 K. The peak energy remains constant, while the excitation density varies for about 2 orders of magnitude.

Table 1. TRPL Decay Time Constants and Amplitude Ratios for the Violet Emission at Different Temperatures[a]

temp/K	τ_1/ns	WF_1/%[b]	τ_2/ns	WF_2/%	$\langle\tau\rangle$/ns
13	129.3	41.66	1138.4	58.34	1062.7
60	104.4	45.66	746.6	54.34	679.1
150	67.8	43.62	493.9	56.38	453.0
190	16.7	46.69	125.8	53.31	114.4
220	6.2	43.81	41.6	56.19	37.9
300	1.6	56.14	9.2	43.86	7.8

[a]The data are derived from fitting of the decay curves to eq 1. The definition of $\langle\tau\rangle$ is according to ref 19. [b]WF_i (weight factor) = $A_i/(A_1 + A_2)$, where i = 1, 2.

analyses in Figure 3b,c, a considerable red shift of the peak from 3.18 to 3.13 eV with delay time can be observed. As we know, different emitting channels have different lifetimes, respectively. The longer lifetime part will gradually dominate the emission with the increased delay time. Therefore, the red shift of the PL peak with delay time here indicated that there should be different emitting channels (at least two channels) with different lifetimes for the violet emission in the H-plasma-treated ZnO. It has been reported that such a red shift can also be a characteristic of donor−acceptor pair (DAP) recombination.[26] However, according to the excitation density-dependent PL spectra in Figure 3d, the violet emission peak does not shift when the excitation density increases for about 2 orders of magnitude. This behavior suggests that the violet emission is not due to DAP because a blue shift of the DAP emission can be observed at higher excitation densities.[27,28]

To further study the mechanism of the violet emission, annealing experiments were carried out. The high-energy (30 W) H-plasma-treated ZnO nanorods were annealed at 200, 300, and 400 °C in vacuum for 1 h, respectively. Figure 4a shows the room-temperature PL spectra of the high-energy (30 W) H-plasma-treated ZnO before and after annealing. It can be found that the PL intensity of the NBE is decreased with increasing annealing temperature. Moreover, the PL spectrum of the sample annealed at 400 °C shows a relatively strong visible emission, showing that the H passivation effect is weakened because large amounts of H evolve out of ZnO at 400 °C. A similar phenomenon was observed by Dong et al.,[21] which can be explained by the outdiffusion of H that occurred in the process of annealing. Figure 4b shows the low-temperature (13 K) PL spectra of high-energy (30W) H-plasma-treated ZnO before and after annealing. It can be seen

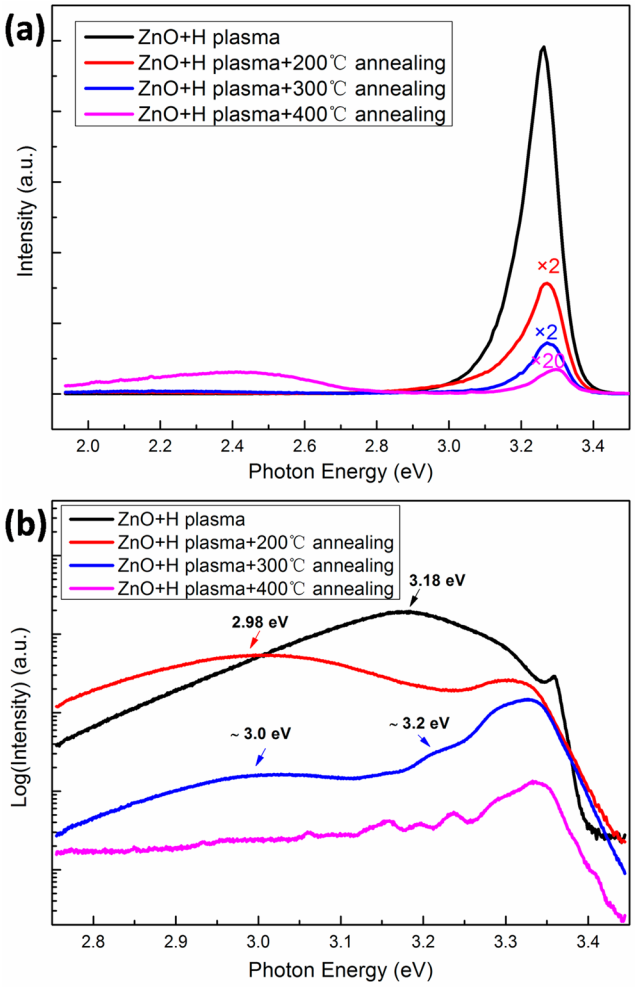

Figure 4. (a) Room-temperature and (b) low-temperature (13 K) PL spectra of the H-plasma-treated (30 W) ZnO nanorods annealed at different temperatures.

that the peak of the violet emission in a 200 °C annealed sample shifts to 2.98 eV, while in a 300 °C annealed sample, two emission lines at about 3.0 eV and 3.2 eV are observed. It can be found that the PL spectra of H-plasma-treated ZnO nanorods annealed at different temperatures exhibit different emission peak positions, respectively, which can be attributed to different emitting channels. The results here are consistent with TRPL analyses, indicating that the violet emission is determined by at least two emitting channels. Moreover, the violet emission almost disappears in a 400 °C annealed sample, while the visible emission appears. Considering that large amounts of H diffusing out of ZnO at 400 °C, there may exist a correlation between the violet emission and H.

Such a strong violet emission at 3.18 eV at 13 K has been rarely reported in ZnO nanorod arrays, and its mechanism has been limited so far. He et al.[29] reported the violet emission at 3.0 eV with unusual fine structures from neon-implanted ZnO nanorods, and they attributed it to acceptor-like defects in ZnO induced by neon implantation. Zeng et al.[30] introduced a high concentration of defects into nanoscale ZnO and observed a dominant blue emission. They thought that the blue emissions were due to Zn_i-related defect levels as initial states. In this work, the violet emission only exists in high-energy (30 W) H-plasma-treated ZnO, while it does not appear in low-energy (20 W) H-plasma-treated ZnO or as-grown ZnO. It seems that the power of H plasma has an impact on the violet emission of ZnO in this work. To confirm this, ZnO nanorods were treated with H plasma of different power (20, 25, 30, and 35 W) for 40 min. PL spectra of the samples treated with H plasma of different power are given (Figure S5 in the SI). The dominant violet emission only appears in ZnO nanorods treated with H plasma of 30 and 35 W. However, the ZnO nanorods treated with H plasma of 25 W only exhibit a relatively broad and weak emission around 3.1 eV. It seems that only when the plasma power is close to or exceeding 30 W, the dominant violet emission can be induced in H-plasma-treated ZnO. Moreover, the PL spectrum of the H-plasma-treated (20 W) ZnO seems to change little except a slight broadening when the treatment time was increased to 2 h. It is widely recognized that large numbers of native point defects are present in as-grown ZnO. It is reasonable to believe that H may be bound to native point defects more easily under high-energy H plasma treatment. Therefore, when the plasma power is close to or exceeding 30 W, more H atoms can be bound to the native point, leading to the formation of a complex defect, resulting in a dominant violet emission, which is consistent with our results. In addition, the violet emission almost disappeared after 400 °C annealing because of escape of H. On the basis of the results above, we suggest that H-related complex defects are formed under high-energy H plasma treatment, which can act as radiative recombination centers, resulting in the violet emission. However, it is difficult for us to accurately identify which complex defect causes the violet emission because of the diversity of the H-related complex defects. We can only determine that the violet emission originated from at least two emitting channels.

CONCLUSIONS

In summary, we show that ZnO nanorod arrays treated with high-energy H plasma exhibited unusual PL features. The low-temperature PL spectrum of the high-energy H-plasma-treated sample was dominated by an extremely strong violet emission around 3.18 eV and a shoulder at 3.36 eV attributed to D^0X. The violet emission showed normal thermal quenching behavior, while the excitonic emission showed NTQ behavior within a temperature range from 110 to 250 K. The violet emission only existed in high-energy (30 W) H-plasma-treated ZnO, while it did not appear in low-energy (20 W) H-plasma-treated or as-grown ZnO. The average lifetime of the violet emission at 13 K is about 1 μs. On the basis of TRPL and excitation density-dependent PL, it was found that the violet emission should be derived from at least two emitting channels, which was confirmed by annealing experiments. The results also gave evidence that the violet emission is related to H. We attributed the violet emission to the H-related complex defects formed under high-energy H plasma treatment. The present study can promote our understanding of the optical properties of ZnO nanostructures, which is a promising building block for nanoscale optoelectronic devices.

ASSOCIATED CONTENT

Supporting Information

Low-temperature and temperature-dependent PL spectra of as-grown and H-plasma-treated (20 W) ZnO nanorods and low-temperature PL spectra of ZnO nanorods treated with H plasma of different power. This material is available free of charge via the Internet at http://pubs.acs.org.

AUTHOR INFORMATION

Corresponding Author

*E-mail: yezz@zju.edu.cn. Tel: +86 571 87952625. Fax: +86 571 87952625.

Author Contributions

The manuscript was written through contributions of all authors. All authors have given approval to the final version of the manuscript.

Notes

The authors declare no competing financial interest.

ACKNOWLEDGMENTS

This work was supported by the National Basic Research Program of China under Grants 51172204, 51072181, 21003105, 51202217, and 51172203 and the Doctoral Fund of Ministry of Education of China under Grants 20110101110028 and 20120101120116.

REFERENCES

(1) Huang, M. H.; Mao, S.; Feick, H.; Yan, H. Q.; Wu, Y. Y.; Kind, H.; Webber, E.; Russo, R.; Yang, P. D. *Science* **2001**, *292*, 1897−1899.
(2) Look, D. C. *Mater. Sci. Eng. B* **2001**, *80*, 383−387.
(3) Xia, Y.; Yang, P.; Sun, Y.; Wu, Y.; Mayer, B.; Gates, B.; Yin, Y.; Kim, F.; Yan, H. *Adv. Mater.* **2003**, *15*, 353−389.
(4) Vines, L.; Wong-Leung, J.; Jagadish, C.; Quemener, V.; Monakhov, E. V.; Svensson, B. G. *Appl. Phys. Lett.* **2012**, *100*, 212106−212106-4.
(5) Yang, Y.; Tay, B. K.; Sun, X. W.; Sze, J. Y.; Han, Z. J.; Wang, J. X.; Zhang, X. H.; Li, Y. B.; Zhang, S. *Appl. Phys. Lett.* **2007**, *91*, 071921−071921-3.
(6) Chen, R.; Ye, Q. L.; He, T. C.; Wu, T.; Sun, H. D. *Appl. Phys. Lett.* **2011**, *98*, 241916−241916-3.
(7) Bera, A.; Ghosh, T.; Basak, D. *ACS Appl. Mater. Interfaces* **2010**, *2*, 2898−2903.
(8) Mahanti, M.; Ghosh, T.; Basak, D. *Nanoscale* **2011**, *3*, 4427−4433.
(9) Ohashi, N.; Ishigaki, T.; Okada, N.; Sekiguchi, T.; Sakaguchi, I.; Haneda, H. *Appl. Phys. Lett.* **2002**, *80*, 2869−2871.
(10) Li, Y. B.; Zhong, M.; Tokizono, T.; Yamada, I.; Bremond, G.; Delaunay, J. J. *Nanotechnology* **2011**, *22*, 435703−435703-6.
(11) Wang, D.; Seo, H. W.; Tin, C. C.; Bozack, M. J.; Williams, J. R.; Park, M.; Sathitsuksanoh, N.; Cheng, A. J.; Tzeng, Y. H. *J. Appl. Phys.* **2006**, *99*, 113509−113509-5.
(12) Kukreja, L. M.; Misra, P.; Fallert, J.; Phase, D. M.; Kalt, H. *J. Appl. Phys.* **2012**, *112*, 013525−013525-10.
(13) Chang, S. S. *J. Korean Ceram. Soc.* **2011**, *48*, 251−256.
(14) Chen, C.; He, H. P.; Lu, Y. F.; Wu, K. W.; Ye, Z. Z. *ACS Appl. Mater. Interfaces* **2013**, *5*, 6354−6359.
(15) Chen, M.; Wang, X.; Yu, Y. H.; Pei, Z. L.; Bai, X. D.; Sun, C.; Huang, R. F.; Wen, L. S. *Appl. Surf. Sci.* **2000**, *158*, 134−140.
(16) Cox, S. F. J.; Davis, E. A.; Cottrell, S. P.; King, P. J. C.; Lord, J. S.; Gil, J. M.; Alberto, H. V.; Vilao, R. C.; Duarte, J. P.; de Campos, N. A.; Weidinger, A.; Lichti, R. L.; Irvine, S. J. C. *Phys. Rev. Lett.* **2001**, *86*, 2601−2604.
(17) Scepanovic, M.; Grujic-Brojcin, M.; Vojisavljevic, K.; Bernik, S.; Sreckovic, T. *J. Raman Spectrosc.* **2010**, *41*, 914−921.
(18) Yadav, H. K.; Screenivas, K.; Gupta, V.; Katiyar, R. S. *J. Raman Spectrosc.* **2009**, *40*, 381−386.
(19) Ozgur, U.; Alivov, Y. I.; Liu, C.; Teke, A.; Reshchikov, M. A.; Dogan, S.; Avrutin, V.; Cho, S. J.; Morkoc, H. *J. Appl. Phys.* **2005**, *98*, 041301−041301-103.
(20) Shalish, I.; Temkin, H.; Narayanamurti, V. *Phys. Rev. B* **2004**, *69*, 245401−245401-4.
(21) Dong, J. J.; Zhang, X. W.; You, J. B.; Cai, P. F.; Yin, Z. G.; An, Q.; Ma, X. B.; Jin, P.; Wang, Z. G.; Chu, P. K. *ACS Appl. Mater. Interfaces* **2010**, *2*, 1780−1784.
(22) Shibata, H. *Jpn. J. Appl. Phys.* **1998**, *37*, 550−553.
(23) Watanabe, M.; Sakai, M.; Shibata, H.; Satou, C.; Shibayama, T.; Tampo, H.; Yamada, A.; Matsubara, K.; Sakurai, K.; Ishizuka, S.; Niki, S.; Maeda, K.; Niikura, I. *Physica B* **2007**, *376*, 711−714.
(24) Hamby, D. W.; Lucca, D. A.; Klopfstein, M. J. *J. Appl. Phys.* **2005**, *97*, 043504−043504-8.
(25) Kamat, P. V.; Patrick, B. *J. Phys. Chem.* **1992**, *96*, 6829−6834.
(26) Reshchikov, M. A.; Xie, J. Q.; Hertog, B.; Osinsky, A. *J. Appl. Phys.* **2008**, *103*, 103514−103514-8.
(27) Stichtenoth, D.; Durr, J.; Ronning, C.; Wischmeier, L.; Voss, T. *J. Appl. Phys.* **2008**, *103*, 083513−083513-5.
(28) Thomas, D. G.; Hopfield, J. J.; Augustyn, W. M. *Phys. Rev.* **1965**, *140*, A202−A220.
(29) Liu, H. B.; He, H. P.; Li, S. L.; Wu, K. W.; Huang, J. Y.; Lu, Y. F.; Pan, X. H.; Ye, Z. Z. *Appl. Phys. Express* **2012**, *5*, 112102−112102-3.
(30) Zeng, H. B.; Duan, G. T.; Li, Y.; Yang, S. K.; Xu, X. X.; Cai, W. P. *Adv. Funct. Mater.* **2010**, *20*, 561−572.